Supporting Information

Self-assembly of coordination polymers on plasmonic surfaces for computer vision decodable, unclonable and colorful security labels

Fei Han, Yang Liu, Fushan Li, Yongfeng Lu, Hongrui Cheng, Yuting Lin, Tiesong Zhao, Soon Hock Ng, Udo Bach, Yuanhui Zheng**

Materials and Methods

Materials

Acetone (AR grade) and ethanol (AR grade) were purchased from Guangdong Guanghua Sci-Tech Co., Ltd). Cupric bromide (99%), pyrazine (98%), H_2O_2 (3% wt in H_2O) and glacial acetic acid (99.7%) were obtained from Energy Chemical (China).

Synthesis of the cupric bromide complexes of pyrazine 1, 4-dioxide: Typically, pyrazine (140.625 mmol, 11.25 g), 40 mL of H_2O_2 (30% wt. % in H_2O) and 90 mL of glacial acetic acid were refluxed at 75 ^oC for 24 h. Subsequently, 500 mL of acetone was added into the above solution to crystallize pyrazine 1, 4-dioxide. The obtained pyrazine 1, 4-dioxide (2.5 mmol, 0.28 g) and cupric bromide ($CuBr_2$) (1.3 mmol, 0.3 g) were dissolved in the Milli-Q water (5 mL). The green crystal, cupric bromide complexes of pyrazine 1, 4-dioxide, was then obtained by the evaporation of water at 120 ^oC.

Fabrication of the security labels

In a typical procedure, a commercially available silicon wafer (purchased from UniversityWafer) was cleaned by immersing it in an acetone bath at 70°C for 3 minutes followed by rinsing with isopropanol and finally dried under a stream of nitrogen. A positive photoresist (AZ 1512HS purchased from AZ Electronics Materials) was first spin-coated on the Si wafer at 3,000 rpm for 30 seconds, soft-baked at 90 °C for 1 minute, exposed to UV light (45 mJ/cm^2) through a chromium mask (MiniFAB Pty.Ltd., Scoresby, VIC, Australia) and finally developed in a 3: 2 mixture of AZ 726 MIF developer (purchased from AZ Electronics Materials) and ultrapure water for 50 seconds. The exposed photoresist was dissolved in AZ 726 MIF solution, yielding a patterned substrate. Subsequently, a Ti(5 nm)/Au(30 nm) layer was deposited on the patterned substrate using an electron-beam evaporator. The obtained wafer was then cut into small pieces of 6 mm × 4 mm. For the self-assembly of cupric bromide complex of pyrazine 1, 4-dioxide on the patterned substrate 5 μL of cupric bromide complex of pyrazine 1, 4-dioxide solution (10 mg/mL) was drop-casted on the substrate and vacuum-dried for 20~30 s. The patterned substrate was then immersed into the acetone at 60 ^oC for 1 minute to lift-off the photoresist. After the lift-off procedure, the substrate was dried under a stream of nitrogen. Finally, the obtained sample was spin-coated with PMMA (1 wt%) chlorobenzene solution and heated at 60 ^{o}C for 10 minutes until it was completely dried.

Characterization

The UV−Vis absorption spectrum was tested with a UV/Vis/NIR spectrophotometer (Shimadzu, UV-3600). The steady-state photoluminescence (PL) spectra were collected with a Hitachi F-4600 fluorescence spectrophotometer, by exciting the samples using a Xe lamp coupled with a monochromator. The dark field, bright field and fluorescence images of PUF patterns morphology were characterized by using a compact microscope (Olympus BX51M). The powder X-ray diffraction (XRD) data are collected on a Bruker D8 ADVANCE X-ray diffractometer with Cu Ka radiation, which operates at 40 kV and 40 mA. The scan rate is 0.5 (2θ s^{-1}). The 3D fluorescence image was obtained by the confocal laser scanning microscope (Olympus LEXT OLS4000). The chemical structures of the coordination polymer and pyzO were recorded on a Nicolet 670 FTIR spectrometer. The images of the sample thickness were obtained by the atomic force microscope (AFM, Bruke, Dimension Icon).

Computer vision authentication approach

A computer vision authentication program (see note S1) that contains Scale-Invariant Feature Transform (SIFT) algorithm and BruteForce Matcher from OpenCV libraries was written in Python 3.6. SIFT is a feature detection algorithm in computer vision to extract the feature vectors in images, which are robust under changes in image scale, location, rotation, illumination, and noise. The BruteForce Matcher is used to match the extracted features between two images. In a typical authentication process, we created a database containing 75 real security labels with file name, a_n (n = 1, 2, 3…..75) (file format: jpg). The keypoint features of these security labels were extracted with the authentication program and saved as a numpy arrays file a_n (n = 1, 2, 3…..75) in the same database (file format: npy). The npy file is used to describe the keypoint features of the image. Once the npy files are created, all the image files can be deleted. When the supplier, distributor and end-users receive a product tagged with a colorful security label, they need to take a photo of the security label (recognized as a new image) and send it to the computer vision engine for keypoint feature extraction and comparison. To demonstrate the concept, the keypoint features extracted from the new images are named as an npy file b_n or c_n ($n = 1, 2, 3$…..), which represents real security labels and fake ones, respectively. Then the computer vision authentication program can automatically output the indexing name, a_n, with a detailed similarity score according to equation (2) in 10 s. We set a similarity threshold as 0.45 to distinguish the real security labels from the fake ones. Only when the authentication output is higher than the threshold, the security label is recognized as real one, otherwise fake one. The computer used is equipped with the CPU (Intel(R) Core(TM) i5-7500 CPU @3.40GHz), the GPU (NVIDIA GeForce GT 730), the RAM (8.0 GB) and HDD Capability (1000 GB). The computer rated power is 350 W. The storage requirement for the computer vision authentication program we wrote and each generated npy file is 2 K Bytes and 350 K Bytes, respectively.

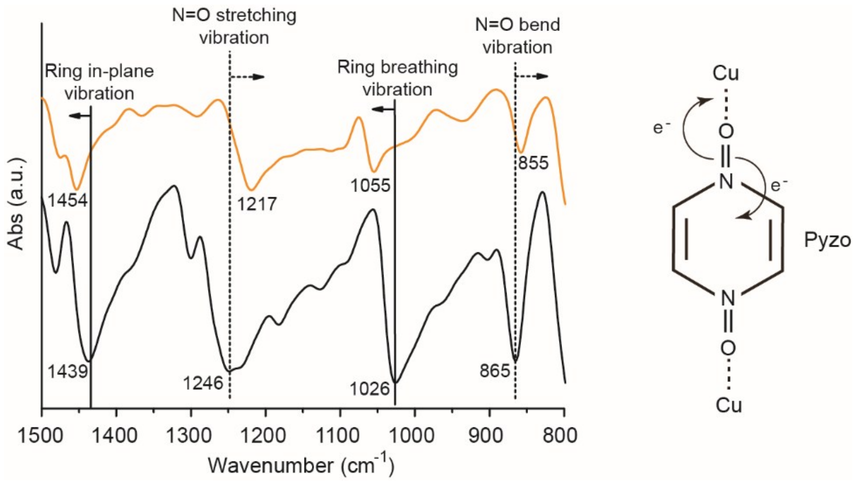

Fig. S1. Fourier transform infrared (FTIR) spectra of pyzO and $CuBr_2(pyzO)(H_2O)_2$ (left) and electron density evolution upon the formation of coordination between copper and pyzo (right). The formation of the O → Cu bond increases the electron demand from the oxygen atom to copper and the electron demand from nitrogen atom to the six-membered ring, corresponding to the reduction of the N=O double-bond strength but the increase of bond strength of all the bonds in the ring. Consequently, the N=O stretching vibration and N=O bend vibration frequencies shift to lower wavenumber, while the ring in-plane vibration and ring breathing vibration peaks to higher wavenumber.[1,2]

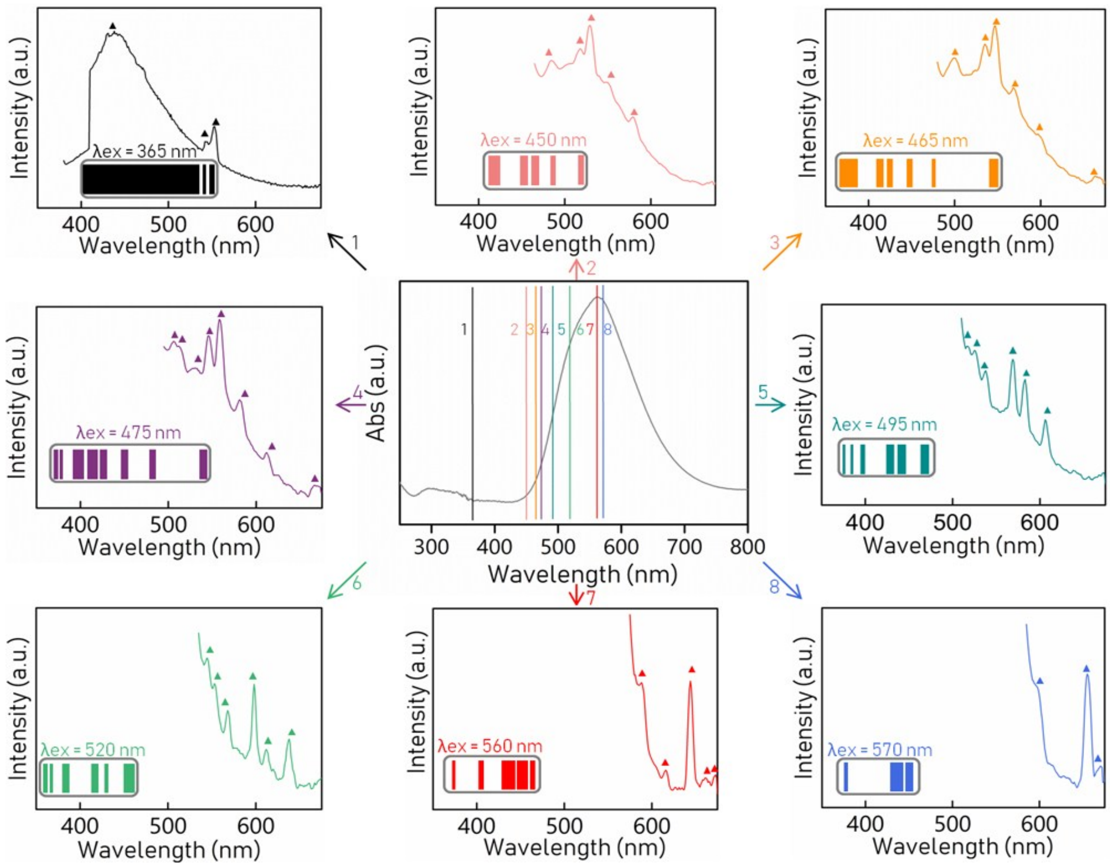

Fig. S2. Excitation-wavelength dependent fluorescence spectra of cupric bromide complexes of pyrazine 1, 4-dioxide and their corresponding fluorescence barcodes (panel 1-8). The excitation wavelength for each fluorescence spectrum is highlighted with a line shown in the absorption spectrum in the middle panel. Each barcode was created by converting all the emission peak widths into a barcode.

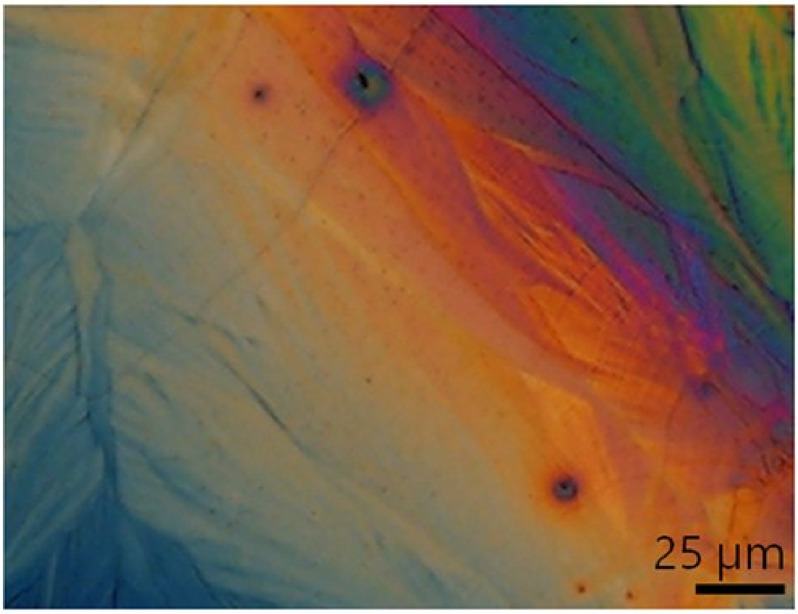

Fig. S3. Typical bright-field image of a coordination polymer crystal (cupric bromide complexes of pyrazine 1, 4-dioxide) on the Si substrate obtained through fast solvent evaporation.

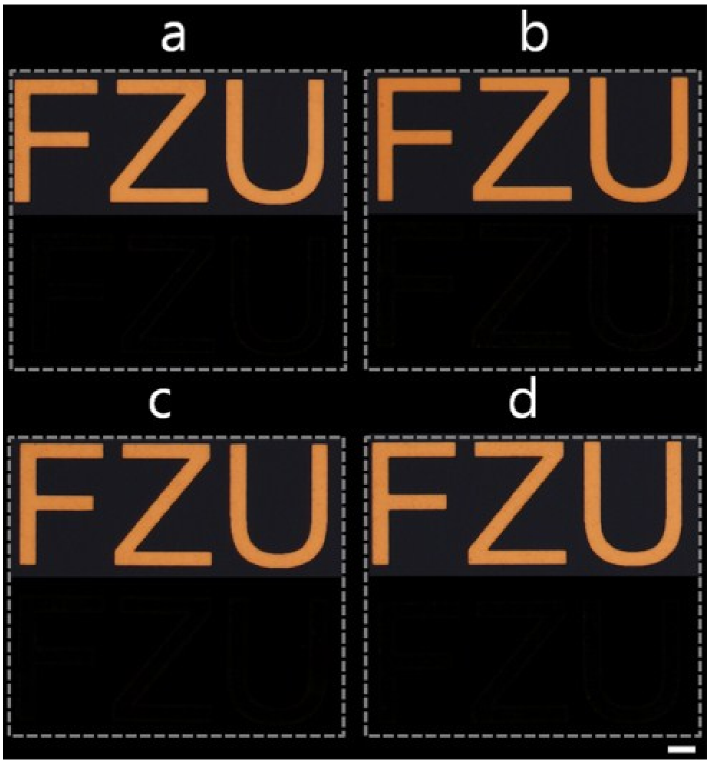

Fig. S4. Four batches of 'FZU' patterns without the PUF tag showing almost identical features: (top) bright-field images and (bottom) dark-field images (scale bar = 50 μm).

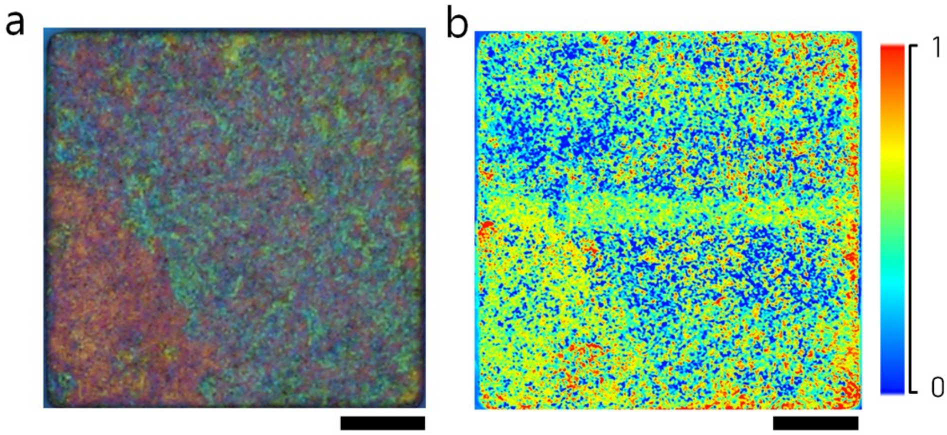

Fig. S5. (a) Bright-field image of a 'square' pattern with the PUF tag, and (b) its corresponding 3D laser scanning image showing the surface topography of the PUF tag (scale bar = 10 μm). The color scale bar provides the height information of the topography. Note that the green-yellow strip in the middle of panel b is caused by the laser heating induced volumetric expansion of the coordination polymers.

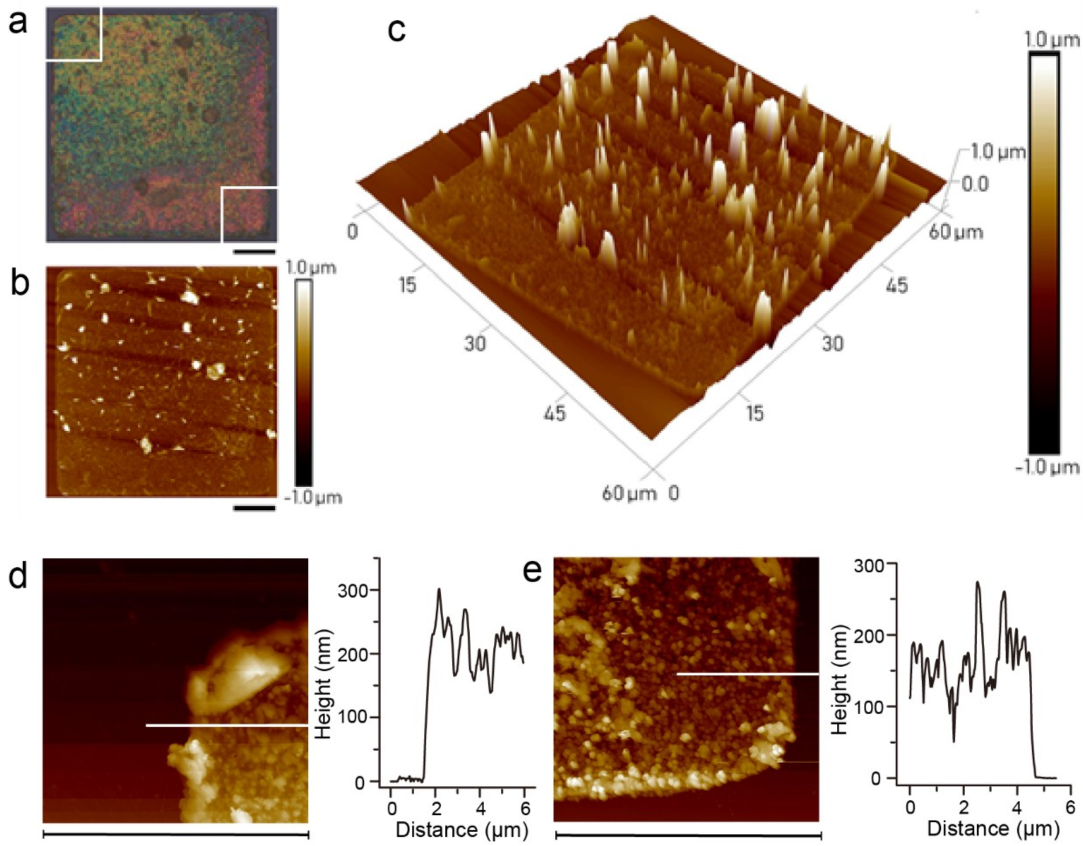

Fig. S6. (a) Bright-field image, (b) 2D and (c) 3D atomic force microscopy (AFM) images of a PUF tag composed of a 'square' pattern, (d) 2D AFM image and its height profile from the top-left corner of the 'square' pattern, and (e) 2D AFM image and its height profile from the bottom-right corner of the 'square' pattern (scale bar = 10 µm). The two selected corners of the 'square' pattern show different colors under bright-field microscope (panel a), which is due to different thicknesses of the coordination polymer layer (panel d and e).

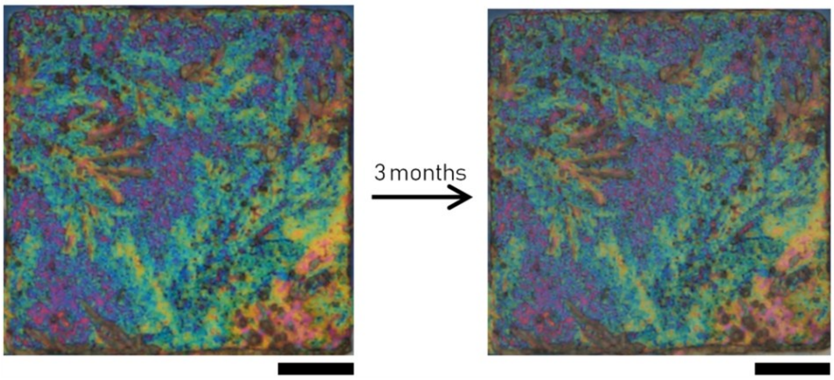

Fig. S7. Photostability of the PUF-based security labels: bright-field image of a square pattern exposed in air for 3 months showing no significant change in color (scale bar: 50 μm).

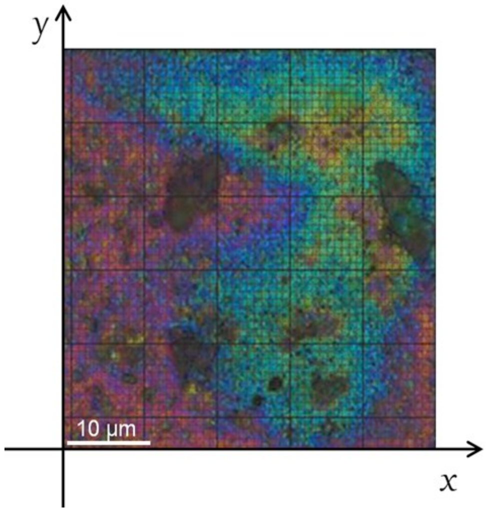

Fig. S8. An example of the encoding capacity estimation of a security label pattern: 50 pixels $\times$ 50 pixels (p = 2500); at least 3 different colors were observed in the pattern (i.e., c $\geq$ 3). Note that in our authentication process, there is no need to define xy axis.

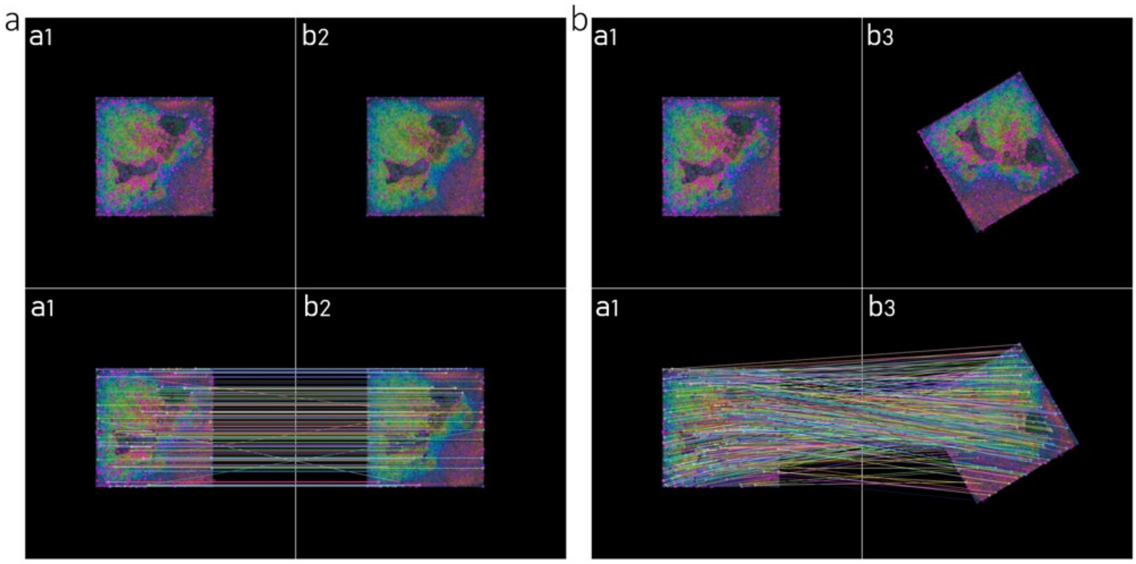

Fig. S9. Examples of feature keypoints matching: the dots represent the feature keypoints, while the lines represent the matched feature keypoints between two images. (a) b_2 vs a_1: N_0 (a_1) = 739, N_t (b_2) = 201, N_m (a_1, b_2) = 186, and S (a_1, b_2) = 0.58893, and (b) b_3 vs a_1: N_0 (a_1) = 739, N_t (b_3) = 700; N_m (a_1, b_3) = 679; S = 0.74897. Note that the similarity (S) was calculated according to equation 2 in the manuscript.

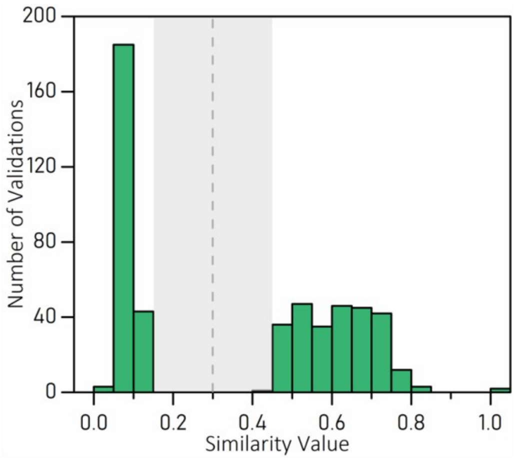

Fig. S10. Histogram of validation events with different similarities to the real security labels in the database. For the Fake security labels, their matching scores are all smaller than 0.15, while the matching scores of the real security labels are higher than 0.45. Note that if the imaging conditions of the real security labels used by the users are identical to those used by the manufacturers, the matching score of the test image will be 1 for all real security labels. In our experiments, only two test images are identical to those in the database, giving matching scores of 1. In order to demonstrate the robustness of our authentication approach, most of the test images from real security labels are taken under different definition, rotation angles, brightness, magnification and the mixture of these factors to reduce the quality of the images. The resulting matching scores are still high enough to be distinguished from those of fake ones using a threshold at the dash line. Further using a software application to control the image quality during acquisition can easily increase the matching scores of the real security labels, making them closer to 1. In this case, the gap between the smallest similarity difference (i.e., the grey area shown in Figure S8) of the real and fake security labels will become larger, thus making it easier to distinguish them.

Supplementary Note 1

The following is the authentication program we wrote:

```
import cv2
import glob
import time

time_start=time.time()

def match(trueimage,testimage):
    sift = cv2.xfeatures2d.SIFT_create()
    img1 = cv2.imread(testimage)
    img2 = cv2.imread(trueimage)
    kp1, des_test = sift.detectAndCompute(img1, None)
    kp2, des_true = sift.detectAndCompute(img2, None)
    bf = cv2.BFMatcher()
    matches = bf.knnMatch(des_test, des_true, k=2)
    good = [ ]
    for m, n in matches:
        if m.distance < 0.8*n.distance:
            good.append([m])
    p = (len(good)/len(des_test) + len(good)/len(des_true))/2
    # print(p)
    return p

thredshold = 0.3
list = [ ]
for img_test in glob.glob("G:¥¥Test¥¥*.tif"):
    max_p = 0
    for trueimage in glob.glob("G:¥¥True¥¥*.tif"):
        p = match(trueimage,img_test)
        if(p >= max_p):
            max_p = p
    print(max_p)
    if(max_p > thredshold):
        list.append([img_test,"True",max_p])
    else:
        list.append([img_test,"Fake",max_p])
print(list)

output = open('D:¥¥anticounterfeiting¥¥Output.xls','w',encoding='gbk')
output.write('Image¥tTrue&Fake(Thredshold=0.4)¥tSimilarity¥n')
for i in range(len(list)):
    for j in range(len(list[i])):
        output.write(str(list[i][j]))
        output.write('¥t')
    output.write('¥n')
output.close()

time_end=time.time()
print('totally cost',time_end-time_start)
```

References

1. J. A. Schlueter, H. Park, G. J. Halder, W. R. Armand, C. Dunmars, K. W. Chapman, J. L. Manson, J. Singleton, R. McDonald, A. Plonczak, J. Kang, C. Lee, M. H. Whangbo, T. Lancaster, A. J. Steele, I. Franke, J. D. Wright, S. J. Blundell, F. L. Pratt, J. deGeorge, M. M. Turnbull and C. P. Landee, *Inorg. Chem.*, 2012, **51**, 2121-2129.
2. S. Kida, J. V. Quagliano, J. A. Walmsley, and S. Y. Tyree, *Spectrochimi. Acta*, 1963, **19**, 189-199.